Mon. Not. R. Astron. Soc. **356,** 295–308 (2005) doi:10.1111/j.1365-2966.2004.08448.x

On the transmission-dominated to reprocessing-dominated spectral state transitions in Seyfert 2 galaxies

M. Guainazzi,[1⋆] A. C. Fabian,[2] K. Iwasawa,[2] G. Matt[3] and F. Fiore[4]

[1]*XMM–Newton Science Operations Center, European Space Astronomy Center, ESA, Apartado 50727, E-28080 Madrid, Spain*
[2]*Institute of Astronomy, Madingley Road, Cambridge, CB3 0HA*
[3]*Dipartimento di Fisica 'E.Amaldi', Università 'Roma Tre', Via della Vasca Navale 84, I-00146 Rome, Italy*
[4]*INAF-Osservatorio Astronomico di Roma, Via di Frascati 33, I-00040, Monteporzio, Italy*

Accepted 2004 September 23. Received 2004 September 13; in original form 2004 May 28

ABSTRACT

We present *Chandra* and *XMM–Newton* observations of a small sample (11 objects) of optically selected Seyfert 2 galaxies, for which *ASCA* and *BeppoSAX* had suggested Compton-thick obscuration of the active galactic nucleus (AGN). The main goal of this study is to estimate the rate of transitions between 'transmission-dominated' and 'reprocessing-dominated' states. We discover one new transition in NGC 4939, with a possible additional candidate in NGC 5643. This indicates a typical occurrence rate of at least $\sim$0.02 yr^{-1}. These transitions could be due to large changes of the obscuring gas column density, or to a transient dimming of the AGN activity, the latter scenario being supported by detailed analysis of the best-studied events. Independently of the ultimate mechanism, comparison of the observed spectral dynamics with Monte Carlo simulations demonstrates that the obscuring gas is largely inhomogeneous, with multiple absorbing components possibly spread through the whole range of distances from the nucleus between a fraction of parsecs up to several hundred parsecs. As a by-product of this study, we report the first measurement ever of the column density covering the AGN in NGC 3393 ($N_{\rm H} \simeq 4.4 \times 10^{24}$ cm^{-2}), and the discovery of soft X-ray extended emission, apparently aligned along the host galaxy main axis in NGC 5005. The latter object most likely hosts an historically misclassified low-luminosity Compton-thin AGN.

Key words: galaxies: active – galaxies: nuclei – galaxies: Seyfert – X-rays: galaxies.

1 INTRODUCTION

In X-rays, obscured active galactic nuclei (AGN) may be classified into 'Compton-thin' and 'Compton-thick', according to the column of absorbing matter covering the active nucleus. The threshold corresponds to a column density $N_{\rm H} \simeq \sigma_{\rm t}^{-1} \simeq 1.5 \times 10^{24}$ cm^{-2}. The fact that Compton-thick Seyfert 2s are a substantial fraction of the whole population of Seyfert 2 galaxies, maybe as high as 50 per cent (Risaliti, Maiolino & Salvati 1999), suggests that the covering fraction of the absorbing matter is large. If a single absorber covers a steady-state active nucleus, the classification of individual objects is not expected to be time dependent. A review of the observational properties of Compton-thick Seyfert 2 galaxies has been recently published by Comastri (2004).

Bona fide Compton-thick Seyfert 2 galaxies are observed in X-rays also at energies lower than the photoelectric cut-off. This X-ray emission is probably due to reprocessing of the nuclear emission by Compton-thick matter surrounding the nucleus (Matt et al. 2000), and/or by hot plasma in the nuclear environment (Kinkhabwala et al. 2002). We define hereafter 'reprocessing-dominated' Seyfert 2 galaxies to be those whose X-ray emission in the *XMM–Newton* energy band ($E \leqslant 15$ keV) is dominated by reprocessing.[1] The common wisdom so far has been to identify reprocessing-dominated Seyferts with Compton-thick AGN. However, very recently transitions between Compton-thin and Compton-thick spectral states have been serendipitously discovered in a few X-ray-bright Seyfert 2 galaxies (Matt, Guainazzi & Maiolino 2003b, and references therein). In UGC 4203, for instance (Guainazzi et al. 2001; Ohno, Fukazawa & Iyomoto 2004), an *XMM–Newton* observation detected a bright (2–10 keV flux $\simeq 9 \times 10^{-12}$ erg cm^{-2} s^{-1}) AGN, with a low-energy photoelectric cut-off (corresponding to $N_{\rm H} \simeq 2 \times 10^{23}$ cm^{-2}). In *ASCA* observations, performed about six years earlier, the weaker continuum and the huge $K\alpha$ fluorescent iron line (equivalent width, EW, $\simeq$1 keV) can be instead best

⋆E-mail: Matteo.Guainazzi@sciops.esa.int

[1] This definition is therefore conceptually different from '(Compton) reflection-dominated' Seyfert 2s, where the emission in the *XMM–Newton* energy band is dominated by Compton-reflection off the far inner side of the absorber. Nevertheless, almost all known 'reprocessing-dominated' AGN are 'Compton-reflection-dominated'.

Table 1. Sample discussed in this paper. $N_{\rm H}$ measurements in this table were performed prior to *Chandra* and *XMM–Newton*, and are listed in Risaliti et al. (1999), except for the measurement in NGC 4945, which is taken from Guainazzi et al. (2000a).

Object	z	$N_{\rm H,Gal}$ (10^{20} cm^{-2})	$F^{b}_{\rm [O\,III]}$	$N^{a}_{\rm H}$ (cm^{-2})	*XMM–Newton* Obs. date	Exposure time pn/MOS or ACIS (ks)	Time span[c] (yr)
NGC 1068	0.004	3.5	1580	$>10^{25}$	29/30 Jul 2000	61.6/66.8	2.5
Circinus	0.0015	56	697	$(4.3\pm^{1.9}_{1.1})\times10^{24}$	6/7 Aug 2001	70.0/76.0	3.5
NGC 5643	0.004	8.3	69	$>10^{25}$	8 Feb 2002	7.1/9.4	4.9
NGC 1386	0.003	1.4	66	$>10^{24}$	29 Dec 2002	13.6/17.0	6.0
NGC 5135	0.014	4.6	61	$>10^{24}$	4 Sep 2001[d]	29.3	6.6
NGC 3393	0.013	6.0	32	$>10^{25}$	5 Jul 2003	10.9/14.2	6.5
NGC 2273	0.006	7.0	28	$>10^{25}$	5 Sep 2003	10.0/12.6	6.5
NGC 5005	0.003	1.1	20	$>10^{24}$	13 Dec 2002	13.1/8.8	7.0
NGC 4939	0.010	3.4	11	$>10^{25}$	03 Jan 2002	11.5/–	5.0
IC 2560	0.010	6.5	>4	$>10^{24}$	29/30 Oct 2000[d]	9.8	3.9
NGC 4945	0.002	15.7	>4	$(4.4\pm^{0.8}_{0.6})\times10^{24}$	21 Jan 2001	19.2/22.2	1.5

Notes. [a]After Risaliti et al. (1999); derived from *ASCA* or *BeppoSAX* observation. [b]In units of 10^{-13} erg cm^{-2} s^{-1}. [c]Minimum distance between the *ASCA*/*BeppoSAX* and the *Chandra*/*XMM–Newton* observation. [d]*Chandra* observation.

explained if the spectrum is dominated by the Compton echo of an otherwise invisible nuclear emission. Such transitions have been observed in both directions, and are normally accompanied by substantial changes in the observed 2–10 keV flux.

This discovery stimulates some fundamental questions on the nature of reprocessing-dominated Seyfert 2 galaxies. These transitions could be due in principle to a change of the intervening absorption. Alternatively, Seyfert 2 X-ray spectral states dominated by reprocessing may represent phases of low- or totally absent activity in the life of an active nucleus, as observed, for instance, in NGC 4051 (Guainazzi et al. 1998), NGC 2992 (Gilli et al. 2000), and NGC 6300 (Guainazzi 2002). In these cases, the observed transitions require a change by at least one order of magnitude of the nuclear activity level.

Transitions between Compton-thin and Compton-thick spectral states have been observed in four Seyfert 2 galaxies so far (see Matt et al. 2003b, and references therein), out of about 40 objects for which multiple X-ray spectroscopic measurements are available (Bassani et al. 1999; Risaliti et al. 2002). However, the 'parent sample' is neither homogeneous nor complete, being substantially biased toward brighter (and therefore less absorbed) objects (see the discussion in Risaliti et al. 1999).

We are carrying on an *XMM–Newton* survey of an optically defined and complete – albeit small – sample of Seyfert galaxies, classified as Compton-thick according to observations prior to the launch of *Chandra* and *XMM–Newton*. The primary goal of this study is to determine the rate of 'transmission-dominated' (i.e. Compton-thin) to 'reprocessing-dominated' transitions,[2] and their typical time-scale on the soundest possible statistical basis. This rate might be related to the duty cycle of AGN phenomena, at least in the local Universe, if these transitions are due to large changes of the overall X-ray AGN energy output (Matt et al. 2003b). The results of this survey are the main subject of this paper.

2 THE SAMPLE

Our objects are extracted from the sample of Risaliti et al. (1999), which includes nearby Seyfert 2 galaxies with *ASCA*/*BeppoSAX* measurements of the X-ray column density. We have restricted our analysis to those objects whose [O III] luminosity is $>10^{-13}$ erg s^{-1}. As Risaliti et al. (1999) discuss, this choice minimizes any bias due to incompleteness. Out of the potential 14 members of our sample, priority 'A' or 'B' *XMM–Newton* observing time has not been allocated to five of them (IC 2560, IRAS 07145, NGC 5135, IC 3639 and UGC 2456). We complement the *XMM–Newton* observations with two objects observed by *Chandra* (IC 2560 and NGC 5135), whose data are available in the public archive. The galaxies discussed in this paper are listed in Table 1. EPIC spectra of four of the objects listed in Table 1 have already been individually published: NGC 1068 (Matt et al. 2004), the Circinus Galaxy (Molendi, Bianchi & Matt 2003), NGC 5643 (Guainazzi et al. 2004a), and NGC 4945 (Schurch, Roberts & Warwick 2002). The *Chandra* observation of IC 2560 is presented by Iwasawa, Maloney & Fabian (2002); the *Chandra* observation of NGC 5135 is discussed by Levenson et al. (2002, 2004). For the remaining five sources (NGC 1386, 3393, 2273, 5005 and 4939) we present here for the first time the results of their *XMM–Newton* observations.

The average distance between the *Chandra*/*XMM–Newton* observation and the latest *ASCA*/*BeppoSAX* observation of the same object is $\simeq$4.9 yr.

In this paper energies are quoted in the source reference frame, errors on the count rate are at the 1σ level, uncertainties on the spectral parameters are at the 90 per cent confidence level for one interesting parameter, upper limits are also at the 90 per cent confidence level, and in the calculation of the luminosities, we adopted a Hubble constant of 70 km s^{-1} Mpc^{-1} (Bennett et al. 2003). Preliminary results of this study are discussed by Guainazzi et al. (2004b).

3 DATA REDUCTION AND ANALYSIS

XMM–Newton data described in this paper were reduced with SAS v5.4.1 (Jansen et al. 2001), using the most updated calibration files available at the moment the data reduction was performed. In this paper, only data from the EPIC cameras (MOS; Turner et al. 2001; pn, Strüder et al. 2001) will be discussed. X-ray images are generally point-like. Deviations from point-like shapes are apparent in NGC 1068 (Matt et al. 2004), the Circinus Galaxy (Molendi et al. 2003), NGC 4945 (Schurch et al. 2002), and NGC 5005 (Section 5). Event lists from the two MOS cameras were merged before accumulation of any scientific products. Single to double (quadruple) events

[2] Although in this paper we will refer to 'transmission-dominated' to 'reprocessing-dominated' transitions, we search for transitions in both directions.

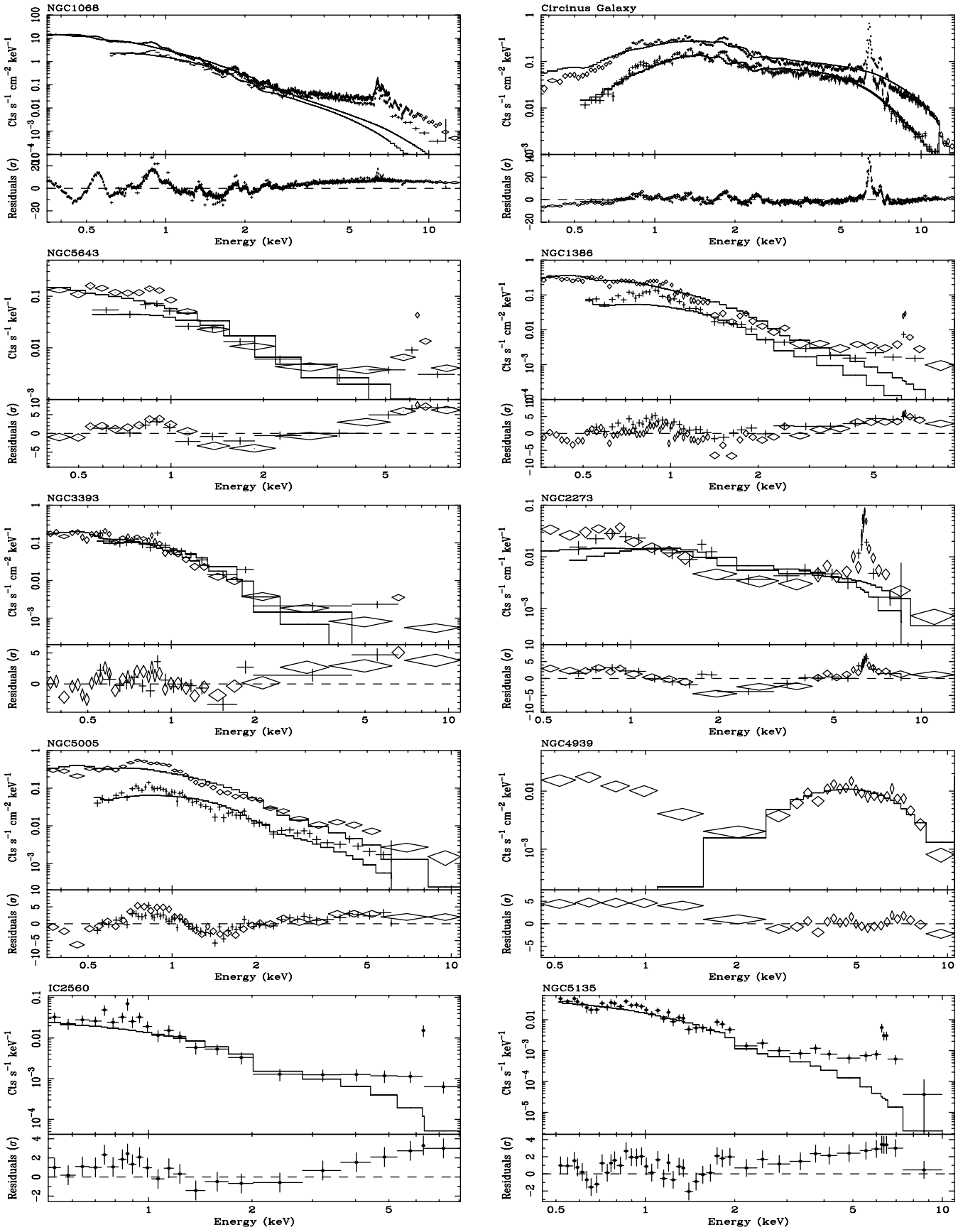

Figure 1. Spectra (upper panels) and residuals against a power-law continuum modified by photoelectric absorption (lower panels) for the *XMM–Newton* and *Chandra* observations of our sample. Readers are referred to Schurch et al. (2002) for NGC 4945. Crosses: MOS; diamonds: pn; dots: ACIS.

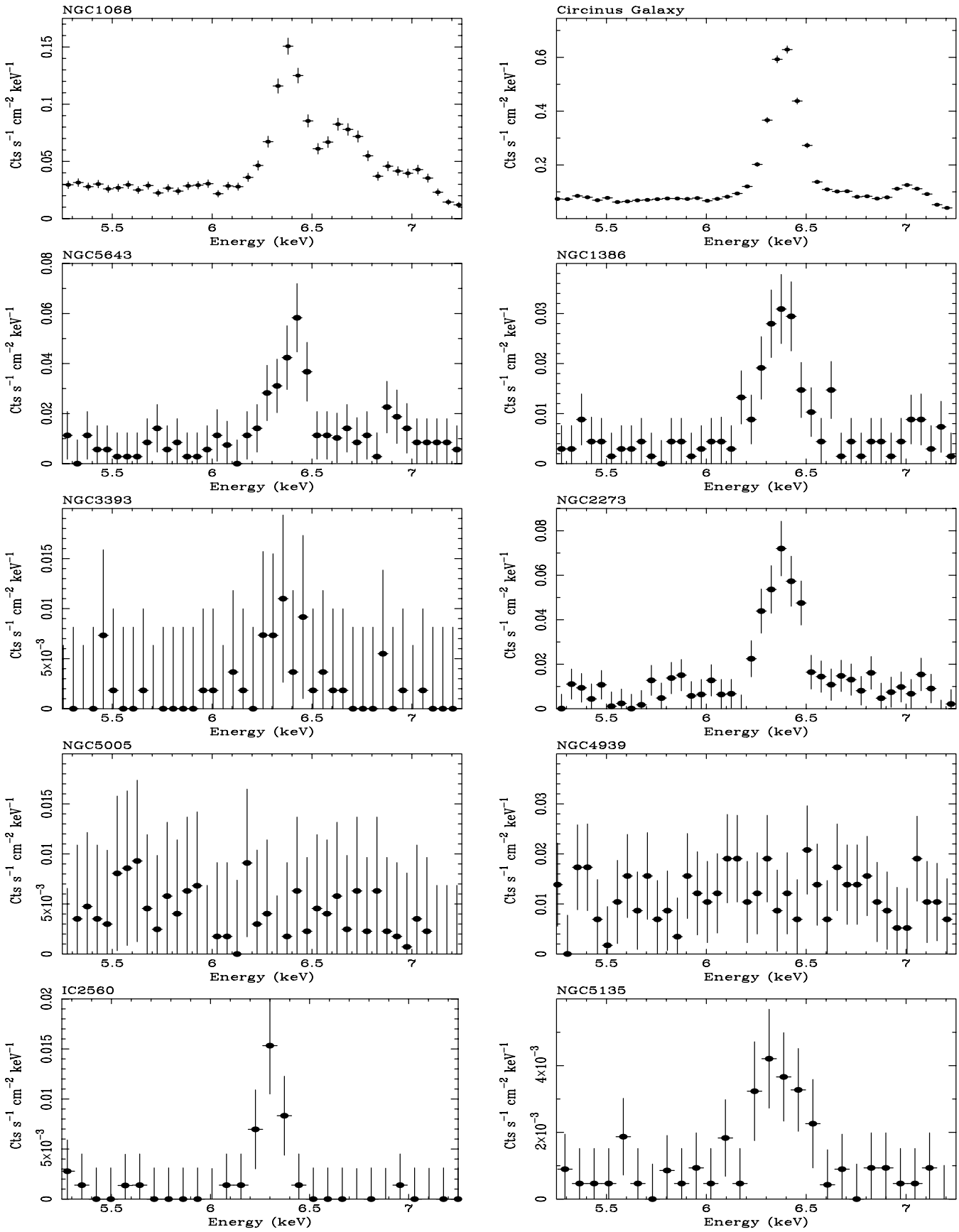

Figure 2. Background-subtracted, linearly rebinned pn and ACIS spectra in the 5.25–7.25 keV energy range for the same objects as in Fig. 1.

were used to accumulate pn (MOS) spectra. High-background particle flares were removed, by applying standard thresholds on the single-event, $E > 10$ keV, $\Delta t = 10$ s, light curves: 1 count s^{-1} and 0.35 count s^{-1} for each pn and MOS camera, respectively. Source spectra were extracted from 40-arcsec circular regions around the X-ray nuclear source centroid, except for NGC 5643 (Guainazzi et al. 2004a), where a smaller region was chosen to avoid a serendipitous nearby bright source. Background scientific products were extracted from annuli around the source for the MOS, and circular regions in the same or nearby chips for the pn, at the same height in detector coordinates as the source location. No significant variations in any energy bands have been observed during the *XMM–Newton* observations presented here for the first time. Spectra were binned in order to oversample the intrinsic instrumental energy resolution by a factor $\geqslant 3$, and to have at least 25 counts in each background-subtracted spectral channel. This ensures that the χ^2 statistics can be used to evaluate the quality of the spectral fitting. pn (MOS) spectra were fitted in the 0.35–15 keV (0.5–10 keV) spectral range.

The residuals of fits against a power-law continuum modified by photoelectric absorption are shown in Fig. 1 for all the sources presented in this paper except NGC 4945 (Schurch et al. 2002). Notwithstanding differences, and despite the large dynamical range in observed flux, the residuals exhibit a remarkably similar pattern. Two continuum components can be distinguished, joining at $\simeq$2 keV (the only exception being the Circinus Galaxy, whose soft X-ray spectrum is heavily absorbed by intervening matter in the plane of our Galaxy). Spectra with the best statistics show emission-like features in the 0.5–1.5 keV energy range (the exceptions being in this case IC 2560, NGC 2273 and NGC 4939, which have the lowest signal-to-noise soft X-ray spectra). Above 2 keV spectra are flat, and exhibit almost ubiquitously intense emission-line features around 6 keV (observer's frame), the only exceptions being NGC 5005 and 4939. The latter feature is most straightforwardly explained as iron $K\alpha$ fluorescence. These lines can be better appreciated in Fig. 2, where we show background-subtracted spectra in the energy range around the $K\alpha$ iron line with a constant linear binning of about 50 eV.

In Section 4 observed spectra will be compared against composite 'two-continuum' scenarios. In these scenarios, the soft X-ray spectrum can be accounted for by one of the following possible model combinations:

(i) emission from an optically thin, collisionally ionized plasma (MEKAL in XSPEC, Mewe, Gronenschild & van der Oord 1985) with free elemental abundances ('thermal scenario' hereafter);

(ii) a power-law with free spectral index $\Gamma_{\rm soft}$, plus as many unresolved emission lines as required according to a 90 per cent confidence level F-test criterion ('scattering scenario').

The hard X-ray continuum will be instead accounted for by one of the following models:

(iii) a power-law with free spectral index $\Gamma_{\rm hard}$, covered by photoelectric absorption with column density $N_{\rm H}$ ('transmission scenario'); and

(iv) a 'bare' (i.e. unabsorbed) Compton-reflection spectrum (PEXRAV in XSPEC; Magdziarz & Zdziarski 1995) with solar abundances ('(Compton) reflection scenario').

These simple parametrizations yield adequate fits for all the spectra presented in this paper. One should, however, be aware of possible limitations inherent to this simple approach. High-resolution spectroscopy of nearby Seyfert 2 galaxies (among which NGC 1068; Kinkhabwala et al. 2002; Brinkman et al. 2002) has convincingly demonstrated that soft X-ray emission is dominated – at least in some cases – by emission lines, with negligible contribution by an underlying continuum. Blending of these emission lines in the EPIC spectra can mimic a continuum emission. This point is discussed to a larger extent by Iwasawa et al. (2003). As our primary concern in this paper is the characterization of the nuclear absorber, the uncertainties induced by a purely phenomenological modelling of the soft X-ray spectrum will not substantially affect the core results of our paper (Guainazzi et al. 2004a). In the above modelling, we exclude moreover the possibility that the reprocessed component dominating the hard X-ray spectrum in the reflection scenario is in turn absorbed – e.g. by the near-side outer rim or atmosphere of the same matter, responsible for reprocessing. This possibility is discussed by Guainazzi et al. (2004a) with respect to the NGC 5643 case. In none of the other sources discussed in this paper have we found convincing evidence for this possibility. However, statistics is often not good enough to strictly rule it out.

4 *XMM–NEWTON*/*CHANDRA* RESULTS

In this section we summarize the results of the *XMM–Newton* and *Chandra* (IC 2560 and NGC 5135) observations of the targets listed in Table 1.

4.1 NGC 1068

NGC 1068 is one of the X-ray brightest and best-studied Compton-thick Seyfert 2 galaxies. Its Compton-thick nature had been suggested by the prominent and multicomponent $K\alpha$ emission-line complex observed by *ASCA* (Ueno et al. 1994; Iwasawa, Fabian & Matt 1997), and finally confirmed by *BeppoSAX* (Matt et al. 1997a). The column density of the absorber covering the active nucleus probably exceeds 10^{25} cm^{-2} (Matt et al. 1997a). The soft X-rays are dominated by line emission following photoionization and photoexcitation by the active nucleus emission (Kinkhabwala et al. 2002), with little contribution from the circumnuclear starburst (Wilson et al. 1992).

The EPIC spectrum of the *XMM–Newton* observation is discussed by Matt et al. (2004). Several Fe and Ni emission lines allowed them to study in detail the nature of the reflecting matter. Detection of the iron $K\alpha$ Compton shoulder confirms that the neutral reflector is Compton-thick. It is likely to be the far-side inner wall of the absorber. Iron (nickel) overabundance of a factor of about 2 (4), for lower Z elements when compared to solar values, was measured as well.

4.2 The Circinus Galaxy

The Circinus Galaxy hosts the closest known active nucleus. *ASCA* unveiled a reprocessing-dominated spectrum (Matt et al. 1996). Detection of the nuclear emission in the PDS instrument onboard *BeppoSAX* (Matt et al. 1999) allowed precise measurements of the column density of the absorber covering the nucleus ($N_{\rm H} \simeq 4 \times 10^{24}$ cm^{-2}). In hard X-rays the nuclear emission is dominated by an unresolved bright core on scales $<$8 pc (Sambruna et al. 2001). The EPIC hard X-ray spectra are discussed by Molendi et al. (2003). Again, the measurement of the iron $K\alpha$ Compton shoulder – previously discovered by *Chandra* (Bianchi et al. 2002) – allowed them to identify matter responsible for the Compton-reflection dominating below 10 keV with the Compton-thick absorber.

4.3 NGC 5643

Maiolino et al. (1998) classified NGC 5643 as a Compton-thick ($N_{\rm H} > 10^{25}\,{\rm cm}^{-2}$) Seyfert 2 galaxy, whose 0.1–10 keV spectrum is dominated by free-electron scattering. However, in a later *XMM–Newton* pointing Guainazzi et al. (2004a) measured a line-of-sight column density in this object, lying between 0.6 and 1.0 $\times\ 10^{24}\,{\rm cm}^{-2}$. The absorber may be directly covering the nuclear emission or its Compton-reflection. Comparison with previous *BeppoSAX* and *ASCA* observations unveiled dramatic changes in the 1–10 keV spectral shape, which can be parametrized as an observed photon index dynamical range $\Delta\Gamma \simeq 2.0$ accompanying a variation of the 2–10 keV flux by a factor >10. The extreme variability observed in the nuclear emission of this object indicates the revival of an AGN which was 'switched-off' during the *BeppoSAX* observation. The interpretation of this large variation is, however, complicated by the fact that the large *ASCA* and *BeppoSAX* apertures ($\simeq$3 arcmin) encompass a bright serendipitous source (christened 'NGC 5643 X-1' by Guainazzi et al. 2004a), apparently located in one of the wide spiral arm of this face-on galaxy. Understanding the spectral dynamics associated with the flux changes requires instruments capable of distinguishing the contribution of the two bright X-ray sources.

4.4 NGC 5135

We have reanalysed the *Chandra* observation already discussed by Levenson et al. (2004). Our results are substantially coincident with theirs. The ACIS-S3 spectrum is best fitted in the 'thermal + reflection' scenario. The soft X-ray spectrum requires two thermal components with $kT \sim 80$ and $\simeq$390 eV, plus an additional emission line with centroid energy $E_{\rm c} \simeq 1.78$ keV. Above 2 keV the spectrum is Compton-reflection dominated, consistent with the AGN being obscured by a column density $N_{\rm H} \gtrsim 9 \times 10^{23}\,{\rm cm}^{-2}$ (for an intrinsic photon index of 1.5 and a reflection fraction $\leqslant$0.5). The intensity of the $K\alpha$ fluorescent emission line is $(5.2\pm^{1.9}_{2.6}) \times 10^{-6}$ photon cm^{-2} s^{-1}, corresponding to an EW against the reflection continuum of $1.7\pm^{0.6}_{0.8}$ keV. The fluxes in the 0.5–2 and 2–10 keV energy bands are $(1.9\pm^{2.8}_{1.0})$ and $(1.6\pm^{1.0}_{0.6}) \times 10^{-13}\,{\rm erg\,cm^{-2}\,s^{-1}}$, respectively.

4.5 NGC 1386

The results of the *XMM–Newton* observation of NGC 1386 are presented for the first time in this paper. Two of the baseline scenarios can be ruled out. The 'scattering + reflection' scenario can be rejected, as it produces a rather bad $\chi^2/\nu = 172.7/83$. The 'thermal + transmission' scenario yields a better fit ($\chi^2/\nu = 131.5/92$). However, it requires a rather flat AGN spectral index ($\Gamma \simeq 0.5$). The two remaining scenarios yield comparably good fits: 'scattering + transmission': $\chi^2/\nu = 135.4/84$; 'thermal + reflection': $\chi^2/\nu = 133.4/94$. In the former, the EW of the $K\alpha$ iron line (EW $\simeq$1.0 keV) is too large with respect to the expected values for transmission through a uniform shell of material encompassing the continuum source (Leahy & Creighton 1993), assuming the best-fitting $N_{\rm H} \simeq 4 \times 10^{23}\,{\rm cm}^{-2}$. In the latter, two thermal components are required to account for the bulk of the soft X-rays, alongside a Compton-reflection component plus iron $K\alpha$ iron line dominating above about 2 keV. The best-fitting parameters for the fits discussed in this section are reported in Table 2. Residuals against the best-fitting models are shown in Fig. 3.

4.6 NGC 3393

NGC 3393 is the object in our sample with the lowest signal-to-noise ratio in the hard X-ray band. The iron line is barely detectable above a very weak continuum, with $\Delta\chi^2/\Delta\nu = 6.2/1$, corresponding to the 98.3 per cent confidence level, if one assumes that the line is predominantly neutral. The scattering scenario yields $\chi^2_\nu \simeq 1.7$. A thermal model for the soft X-ray spectra produces a significantly better fit. In the hard X-ray band, transmission- and reflection-dominated scenarios yield statistically comparable fits. In the former scenario the EW of the $K\alpha$ iron line (EW = 440 ± 180) is about one order of magnitude larger than expected from the measured column density [$N_{\rm H} = (7\pm^{7}_{4}) \times 10^{22}\,{\rm cm}^{-2}$, if $\Gamma \equiv 1.9$]. We conclude therefore that Compton-reflection dominance is the most plausible explanation for the hard X-ray spectrum in this object. The lower limit on the column density covering the active nucleus derived from the *XMM–Newton* observation [$N_{\rm H} > 7\ (9) \times 10^{23}\,{\rm cm}^{-2}$ if $\Gamma = 1.6\ (1.9)$] strictly speaking does not rule out an – albeit

Table 2. Best-fitting parameters and results for the sources in Table 1, whose *XMM–Newton* EPIC spectral fitting results are presented for the first time in this paper. The legend for the 'Model' column two-letter code is as follows: the first letter indicates the scenario that best accounts for the soft X-ray spectrum: scattering ('S'), or thermal emission ('T'); the second letter indicates the scenario that best accounts for the hard X-ray spectrum: transmission ('T'), or reflection ('R').

		Hard X-ray continuum		Emission lines			Soft X-rays			
Source	Model	$\Gamma_{\rm hard}$	$N^a_{\rm H}$ ($10^{23}\,{\rm cm}^{-2}$)	$E_{\rm c}$ (keV)	$I^b_{\rm c}$	EW (keV)	kT (keV)	Z ($Z_\odot$)	$\Gamma_{\rm soft}$	χ^2/ν
NGC 1386	TR	$2.5\pm^{0.5}_{0.4}$	$\geqslant$22	$6.41\pm^{0.02}_{0.03}$	$0.81\pm^{0.16}_{0.14}$	$1.8\pm^{0.4}_{0.3}$	$0.12\pm^{0.05}_{0.02}$	0.07 ± 0.02	...	133.4/94
							0.66 ± 0.03	$\equiv Z(0.12\ {\rm keV})$		
NGC 3393	TR	1.6 ± 1.2	$\geqslant$9	6.4[c]	0.25 ± 0.14	1.4 ± 0.8	$0.14\pm^{0.04}_{0.03}$	$0.04\pm^{0.03}_{0.02}$	...	55.8/43
				$1.84 \pm^{0.12}_{0.04}$	0.15 ± 0.09		$0.57\pm^{0.06}_{0.08}$	$\equiv Z(0.14\ {\rm keV})$		
NGC 2273	TR	1.5 ± 0.4	$\geqslant$18	6.400 ± 0.010	$2.3\pm^{0.4}_{0.3}$	$2.2\pm^{0.4}_{0.3}$	0.8 ± 0.2	<0.06	...	55.2/51
NGC 5005	TT	$1.6\pm^{0.7}_{0.6}$	0.3 ± 0.2	6.4[c]	<0.14	<0.24	$0.60\pm^{0.03}_{0.02}$	$0.30\pm^{0.14}_{0.30}$	...	126.4/122
							$2.3\pm^{1.1}_{0.7}$	$\equiv Z(0.60\ {\rm keV})$		
NGC 4939	ST	1.5±0.5	$1.5 \pm^{0.4}_{0.5}$	6.4[c]	<0.4	<0.07	...	...	2.7 ± 0.4	21.1/21
				6.96[c]	<1.1	<0.21				

Notes. [a]Calculated assuming Γ frozen to its best-fitting value for Compton-reflection dominated spectra, and a reflection fraction $\leqslant$0.5. [b]In units of 10^{-5} photon cm^{-2}. [c]Frozen.

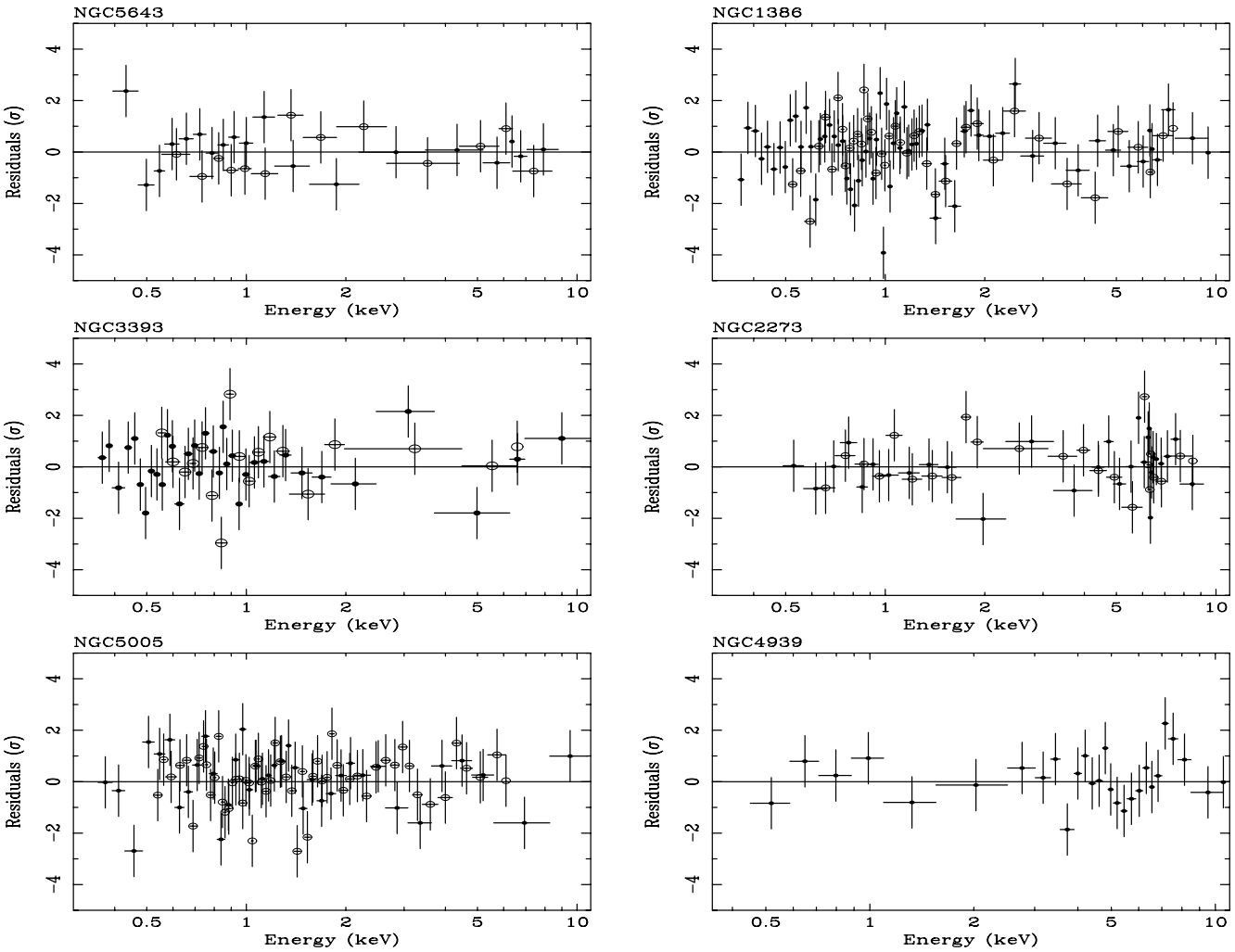

Figure 3. Residuals in units of standard deviations against the best-fitting models as in Table 2, plus NGC 5643; pn: filled dots; MOS: empty circles.

extreme – Compton-thin absorber. None the less, its ultimate nature is confirmed by a reanalysis of the *BeppoSAX* observation (cf. Section. 5). An emission line with centroid energy $E_c \simeq 1.8$ keV is required at the 95.1 per cent confidence level ($\Delta\chi^2/\Delta\nu = 8.4/2$). This line may correspond to $K\alpha$ fluorescence of Si, which is expected to be produced by Compton-reflected spectra. However, its EW against the reflected continuum is ∼5 keV, too large to be produced by the same Compton-reflection responsible for the iron emission (Matt, Fabian & Reynolds 1997b).

4.7 NGC 2273

For NGC 2273 the family of models where hard X-rays are accounted for by an absorbed power law yield an unacceptably flat intrinsic spectral index ($\Gamma \simeq -0.2$–0.5), as well as an unacceptably large EW of the $K\alpha$ iron line (EW $\simeq$ 2.3–3.6 keV) with respect to the measured column density ($N_H \simeq 1.4$–12×10^{22} cm^{-2}). Compton-reflection domination is a viable alternative. Modelling the soft X-rays with the thermal or the scattering scenario makes very little difference on the properties of the hard X-ray continuum or of the $K\alpha$ iron line, although in the latter scenario the photon index best-fitting value is closer to standard values for AGN ($\Gamma \simeq 1.5$ versus 1.2, respectively). In Table 2 we list the results obtained with the former.

4.8 NGC 5005

The *XMM–Newton* observation shows that the X-ray emission is extended, and apparently elongated along a direction close to the main axis of the host galaxy, or coincident with an inner spiral arm, visible in the simultaneous OM UVW1 filter (2500–4000 Å) image (Fig. 4). Although the diffuse emission is mostly associated with soft X-rays, the statistics is not good enough to estimate a threshold energy, above which the X-ray emission is no longer extended. Assuming that the diffuse emission is due to shocked gas in regions of intense star formation, we have considered only models where at least part of the soft X-rays are due to a thermal component. Hard X-ray Compton-dominance is unlikely. A fit where the hard X-ray emission is due to a 'bare' Compton-reflection yields a very steep intrinsic spectral index ($\Gamma_{hard} \simeq 3.1$). Moreover, no iron $K\alpha$ fluorescent line is detected, and the upper limit on the EW of a 6.4-keV narrow Gaussian profile is rather strict ($\leqslant$240 eV). Transmission through a moderate absorber ($N_H \simeq 3 \times 10^{22}$ cm^{-2}) is a viable alternative. The soft X-rays can be accounted for by the combination of two thermal components ($\chi^2/\nu = 126.4/122$) or of one

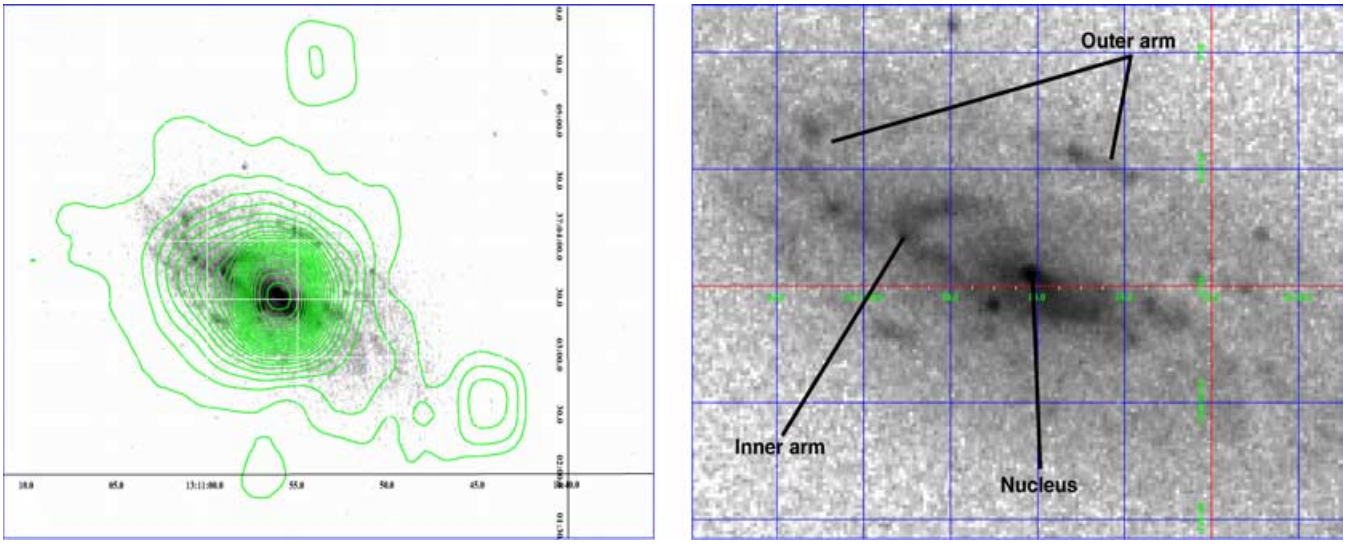

Figure 4. Left-hand panel: pn intensity contours in the 0.2–15 keV energy band superposed on the OM exposure with the UVW1 filter for NGC 5005. The pn image is smoothed with a 6-arcsec kernel boxcar function. Contours represent 15 logarithmically equispaced count levels from 0.17 to 18.29 on the smoothed image. Right-hand panel: zoom of galaxy surface in the UVW1 filter. The position of the nucleus, and of the inner and the outer arms are labelled. The image is 5.25×3.5 arcmin^2.

thermal component and a scattered power-law ($\chi^2/\nu = 138.9/124$). In Table 2 we show the results obtained in the former scenario. In the latter, $\Gamma_{\rm hard} \simeq 1.8$ and $N_{\rm H} \simeq 5 \times 10^{22}$ cm^{-2}.

4.9 NGC 4939

NGC 4939 was serendipitously located in the pn field of view of an observation of SAX J1305.2–1020. Its spectrum is the only one in our sample that clearly exhibits a soft photoelectric cut-off (cf. Fig. 1). Indeed, the transmission scenario accounts well for the hard X-rays, with $N_{\rm H} \simeq 1.5 \times 10^{23}$ cm^{-2}. Modelling the soft X-rays with a single thermal component ($kT \simeq 0.7$ keV) or a steep power law ($\Gamma \simeq 2.7$) yields fits of equivalent statistical quality: $\chi^2/\nu = 18.9/20$ and $21.1/21$, respectively. The best-fitting parameters and results for the latter are shown in Table 2. An emission line is additionally required at the 94.0 per cent confidence level only ($\Delta\chi^2/\Delta\nu = 5.4/2$). Its centroid energy is inconsistent with emission from neutral iron: $E_{\rm c} = 6.71\pm^{0.12}_{0.20}$ keV. If, following Maiolino et al. (1998, cf. Section 5 as well), we interpret this shift of the centroid energy as due to a blend of neutral and H-like transitions, the 90 per cent upper limits on the EW of either component are 70 eV and 210 eV, respectively.

4.10 NGC 4945

The *XMM–Newton* observation of NGC 4945 is discussed by Schurch et al. (2002). The galaxy core has a complex morphology. It is dominated by reprocessing, as the nucleus is covered by a thick absorber ($N_{\rm H} \simeq 4 \times 10^{24}$ cm^{-2}; Done, Madejski & Smith 1996). Compton-reflection from the inner side of an edge-on torus leaves its imprint in the hard X-ray spectrum through a 1.6-keV EW $K\alpha$ emission line, consistent with previous findings (Guainazzi et al. 2000a; Madejski et al. 2000). In soft X-rays, multitemperature emission from a nuclear starburst dominates, a two-temperature model yielding $kT \simeq 0.9$ keV and $kT \simeq 6.9$ keV. The hard X-ray emission exhibits a resolved morphology, suggesting that part of the gas in the starburst region is exposed to the AGN radiation as well.

4.11 IC 2560

IC 2560 has not been observed by *XMM–Newton*. The results of a *Chandra* observation of this target are discussed by Iwasawa et al. (2002). A model constituted by a two-component thermal emission plus a Compton-reflection-dominated spectrum (with $\Gamma \equiv 1.9$) is an adequate description of the spectrum ($\chi^2/\nu = 61.2/74$). The EW of the $K\alpha$ iron line is $\simeq$3.5 keV. In principle, a statistically equivalent fit is obtained if the bare Compton-reflection component is replaced by an absorbed power law ($\chi^2/\nu = 59.9/73$). However, in this scenario the $K\alpha$ iron line EW ($\simeq$8.0 keV) is almost two orders of magnitude too large than expected in transmission from the measured column density ($N_{\rm H} \simeq 5 \times 10^{22}$ cm^{-2}). The *Chandra* observation therefore supports the interpretation of the IC 2560 *ASCA* spectrum as hard X-ray reprocessing-dominated (Risaliti, Maiolino & Bassani 2000), against the interpretation of the same data in terms of a Compton-thin absorber covering the nuclear emission given by Ishihara et al. (2001)

4.12 Fluxes and luminosities

In Table 3 we present the observed fluxes in the 0.5–2 keV and 2–10 keV energy ranges for all the sources in Table 2. The corresponding luminosity corrected for Galactic absorption in the soft X-ray band ranges between 10^{40} and 10^{42} erg s^{-1} (cf. Fig. 10 below). In the hard X-ray band, the determination of the intrinsic AGN luminosity is impossible for all cases where only lower limits on the nuclear absorbing column density exist. For Compton-thick sources they are anyhow plagued by large uncertainties. For the two sources which are Compton-thin in *XMM–Newton* observations, the 2–10 keV luminosity is 1.8×10^{42} erg s^{-1} (NGC 4939), and 1.2×10^{40} erg s^{-1} (NGC 5005), respectively.

5 COMPARISON WITH *ASCA*/*BEPPOSAX* RESULTS

In this section we compare the results of the *Chandra* and *XMM–Newton* observations described in Section 4 with prior *ASCA* and

Table 3. Best-fitting parameters and results for the best fit to the *BeppoSAX* spectra of NGC 4939. Details in text.

$\Gamma_{\rm hard}$	$1.90\pm^{0.16}_{0.19}$
$\Gamma_{\rm soft}$	$3.5\pm^{0.4}_{0.5}$
$N_{\rm H}$ (10^{24} cm^{-2})[a]	>2
0.5–2 keV flux[b]	$0.43\pm^{0.14}_{0.15}$
2–10 keV flux[b]	1.6 ± 0.2
Fe $K\alpha$ lines:	
$I_{\rm c,6.4}$[c]	1.1 ± 0.6
EW$_{\rm c,6.4}$ (eV)	490 ± 270
$I_{\rm c,6.96}$[c]	$1.2\pm^{0.6}_{0.7}$
EW$_{\rm c,6.96}$ (eV)	$460\pm^{270}_{230}$
χ^2/ν	45.4/55

Notes. [a]Assuming $\Gamma_{\rm hard} \equiv 1.9$. [b]In units of 10^{-12} erg cm^{-2} s^{-1}. [c]In units of 10^{-5} photon cm^{-2}.

Table 4. Observed fluxes for the sources listed in Table 2. Units are in 10^{-12} erg cm^{-2} s^{-1}.

Source	0.5–2 keV	2–10 keV
NGC 1386	$1.8\pm^{0.9}_{0.5}$	0.27 ± 0.05
NGC 3393	$0.43\pm^{0.39}_{0.18}$	$0.09\pm^{0.06}_{0.04}$
NGC 2273	$0.12\pm^{0.18}_{0.06}$	$0.69\pm^{0.16}_{0.12}$
NGC 5005	0.47 ± 0.03	0.51 ± 0.06
NGC 4939	0.12 ± 0.04	$3.3\pm^{0.10}_{0.30}$

BeppoSAX measurements. All the spectra described in this section were extracted from calibrated and linearized event lists available in the public archive, and reanalysed by us. Whenever more than one observation was available for a given source, we have considered the latest (in no case was significant spectral variability observed across different *ASCA*/*BeppoSAX* observations, with the only exception of NGC 1068 – Colbert et al. 2002; Guainazzi et al. 2000b). This exception does not substantially affect any of the results discussed in this paper.

Variability in the soft (0.5–2 keV) and hard (2–10 keV) X-ray flux is generally restricted to a factor of ± 3 (Guainazzi et al. 2004b). The intensities (but not the EWs: see Section 6 below) of the $K\alpha$ iron lines are consistent with a factor ± 2 as well. The only exception is NGC 3393 (cf. Table 2, and Table 4), where a delay in the response of a variable primary continuum probably occurs.

In the following, some additional details are given on the analysis of the *ASCA*/*BeppoSAX* observations, whenever our analysis reaches further or different conclusions with respect to what has been published in the literature, or shown by the *XMM–Newton* observations.

5.1 NGC 5135

The absorption-corrected 0.5–2 keV flux during the 1995 January *ASCA* observation was $(1.2\pm^{3.2}_{0.8}) \times 10^{-12}$ erg cm^{-2} s^{-1}. At face value this is one order of magnitude larger than measured by *Chandra* 6.6 yr later. However, the difference is at the 1σ level only, if the statistical uncertainties are taken into account. The other spectral parameters are consistent with the *Chandra* results, with large errors.

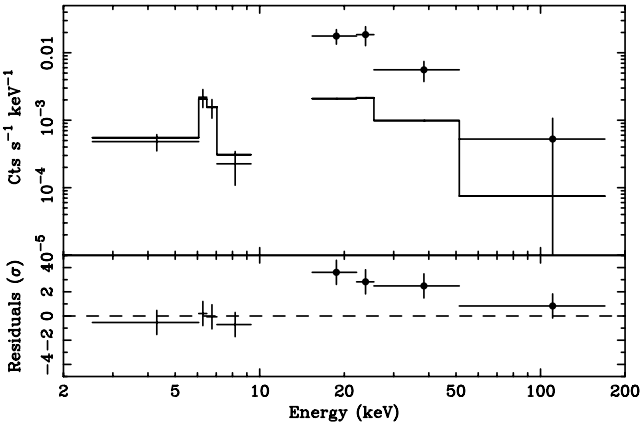

Figure 5. Spectra (upper panel) and residuals in units of standard deviations (lower panel) when the *XMM–Newton* best-fitting spectrum is applied (with $\Gamma \equiv 1.6$) to the *BeppoSAX* spectra of NGC 3393 (MECS: crosses; PDS: filled dots).

5.2 NGC 3393

NGC 3393 is one of the few targets in our sample that was detected by the PDS instrument onboard *BeppoSAX* above 15 keV (count rate: 0.39 ± 0.09 s^{-1}). The *BeppoSAX* observation is discussed by Maiolino et al. (1998). They interpret the *BeppoSAX* spectrum as due to a Compton-thick source, with a column density $>10^{25}$ cm^{-2}. The overall poor statistics of the *BeppoSAX* observation prevented them from applying more complex models. However, the PDS data points in their fig. 1 lay systematically above the extrapolation of the best-fitting model in the 2–10 keV band.

We have first applied the best model of the *XMM–Newton* observation to the *BeppoSAX* spectra. As NGC 3393 is undetected by the LECS instrument below 2 keV, we kept the parameters of the thermal components and of the $E_{\rm c} \simeq 1.8$ keV emission line frozen to the *XMM–Newton* best-fitting values, as the contribution of these components is negligible in the MECS-PDS energy bandpass. The best-fitting intrinsic spectral index face value turns out to be $\Gamma \simeq 0.7$. Although the quality of the fit is acceptable ($\chi^2/\nu = 21.4/17$), this flat index – still consistent with the *XMM–Newton* results within the large statistical uncertainties – is suggestive of additional spectral complexity. If Γ is fixed to the *XMM–Newton* best-fitting value (1.6), the PDS counts are largely underpredicted (Fig. 5).

The difference is even larger if more typical values $\geqslant 1.9$ are used. We conclude that the flux in the PDS band is dominated by the nuclear emission piercing through a Compton-thick absorber, with $N_{\rm H} < 10^{25}$ cm^{-2}. Adding an absorbed power law to the *XMM–Newton* best-fitting model yields an improvement in the quality of the fit at the 96.7 per cent confidence level ($\Delta\chi^2/\Delta\nu = 7.8/2$), with $N_{\rm H} \sim 4 \times 10^{24}$ cm^{-2}, and a slightly steeper intrinsic spectral index. The best-fitting parameters are shown in Table 5. These results confirm that the column density covering the NGC 3393 nucleus is indeed Compton-thick, although not large enough to suppress the nuclear emission fully.

Table 5. Best-fitting parameters and results when the *XMM–Newton* model (expanded with a power-law covered by an absorber of column density $N_{\rm H}$ to account for the emission in the PDS energy band) is applied to the *BeppoSAX* spectra of NGC 3393. Details in text.

Γ	$2.8\pm^{1.2}_{0.7}$
$N_{\rm H}$ (10^{24} cm^{-2})	$4.4\pm^{2.5}_{1.1}$
Fe $K\alpha$ line:	
$E_{\rm c}$ (keV)	$6.58\pm^{0.18}_{0.21}$
$I_{\rm c}{}^{a}$	1.4 ± 0.8
EW (keV)	4 ± 2
χ^2/ν	13.6/15

Note. [a]In units of 10^{-5} photon cm^{-2}.

5.3 NGC 4939

NGC 4939 was classified as a Compton-reflection dominated Compton-thick AGN by Maiolino et al. (1998), on the basis of the very flat spectral index obtained in the 'transmission-scenario', and the fact that this model underpredicts the emission in the PDS band (13–200 keV count rate: 0.20 ± 0.06 s^{-1}). We have reanalysed the same data, obtaining results which are basically consistent with theirs. The EW of a single Gaussian profile accounting for the observed iron emission line ($\simeq$750 eV) is indeed too large with respect to the measured column density in the transmission scenario ($N_{\rm H} \simeq 1.3 \times 10^{23}$ cm^{-2}). A fit where hard X-rays are dominated by a bare Compton-reflection is excellent ($\chi^2/\nu = 45.4/55$; Table 5). The reflection-dominated state is confirmed by the large EW of the neutral component of the iron $K\alpha$ fluorescent line (EW $\simeq$ 500 eV). The H-like component exhibits a comparable EW. The combination of hard X-ray continuum and iron emission-line EW points to a transition between a reprocessing- and a transmission-dominated state occurring between the 1997 January *BeppoSAX* and the 2001 March *XMM–Newton* observations. A comparison between the 3–10 keV spectral energy distribution, based on the best-fitting *BeppoSAX* and *XMM–Newton* models, is shown in Fig. 6.

It is interesting to observe that the soft ($E \leqslant 2$ keV) X-ray flux *decreased* by a factor $\simeq$3.5 between the *BeppoSAX* and the *XMM–Newton* observation. This supports our interpretation of the soft X-ray emission in this object as due to scattering of the primary nuclear continuum, which was mirroring a previous phase of strong AGN activity during the *BeppoSAX* observation. However, the fact that $\Gamma_{\rm soft} \simeq 3.5$ is significantly steeper than $\Gamma_{\rm hard}$ suggests that other components (discrete sources, unresolved diffuse emission) contribute as well in the large *BeppoSAX* aperture.

5.4 NGC 5005

NGC 5005 was declared Compton-thick by Risaliti et al. (1999) on the basis of the low X-ray versus O[III] luminosity ratio, although no evidence for either a flat hard X-ray spectrum or for a $K\alpha$ iron line was observed in the *ASCA* spectrum. The upper limit of the EW of the latter feature (900 eV) was still consistent with heavy obscuration. None of the criteria adopted to classify this source as a Compton-thick object resists scrutiny after the *XMM–Newton* observation. The upper limit on the $K\alpha$ iron line EW is strict (<240 eV). The application of the best-fitting *XMM–Newton* model (cf. Table 2) to the *ASCA* data yields a good fit ($\chi^2/\nu = 216.1/227$), showing that the *ASCA* data have not enough statistics to distinguish a transmission- from a reprocessing-dominated scenario on the basis of the X-ray continuum shape. Literature measurements of the O[III] flux – once corrected for optical reddening using the prescription in Bassani et al. (1999) – span a rather large interval, between 0.3 and 20×10^{-13} erg cm^{-2} s^{-1} (Shuder & Osterbrock 1981; Dahari & De Robertis 1988; Ho et al. 1997; Risaliti et al. 1999). This interval is consistent with 2–10 keV versus O[III] ratio values observed in Compton-thin as well as Compton-thick Seyfert 2s (Fig. 7). We therefore conclude that NGC 5005 is most likely a misclassified Compton-thin Seyfert 2.

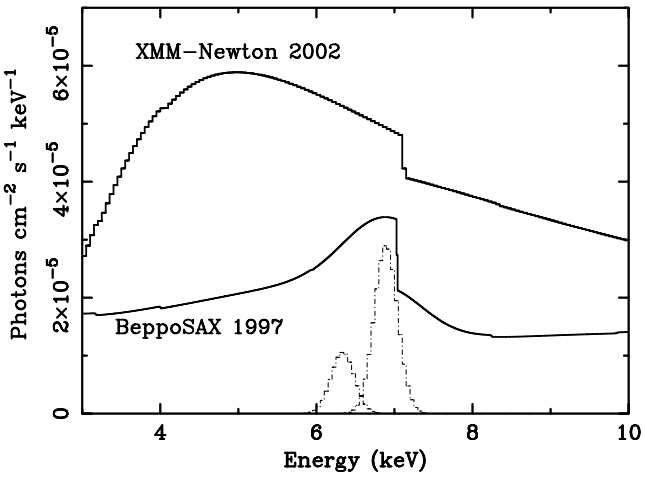

Figure 6. 3–10 keV total spectral energy distributions of NGC 4939 based on the 1997 *BeppoSAX* and 2002 *XMM–Newton* observations (solid lines). The dot–dashed lines indicate the upper limits for the 6.4-keV and 6.96-keV $K\alpha$ fluorescent emission lines in the *XMM–Newton* observation. For display purpose only, we have attributed to all emission lines a formal width equal to the intrinsic instrumental energy resolution: 150 eV and 500 eV for *XMM–Newton* (pn) and *BeppoSAX* (MECS), respectively.

6 DISCUSSION

6.1 How much do we know of Compton-thick Seyfert 2 galaxies?

The safest way to identify a Compton-thick Seyfert 2 galaxy, and describe – even at the simplest phenomenological level – the basic X-ray properties of its nuclear emission is to detect the primary continuum piercing through the Compton-thick absorber. This requires measurements above 10 keV, which have been possible so far only on the $\sim$10 objects detected by the PDS instrument onboard *BeppoSAX* (Matt et al. 2001; Comastri 2004). For all the remaining known $\simeq$30 Compton-thick Seyfert 2s (Comastri 2004) the classification relies on indirect evidence, such as the flatness of the hard X-ray continuum, the EW of the $K\alpha$ iron fluorescent emission line(s), or anomalous low values of the ratio between the flux in the 2–10 keV energy band and in other wavelengths.

Waiting for an X-ray detector of better (>10 keV) sensitivity than the PDS, the robustness of the criteria used to identify Compton-thick objects can be tested with the improved sensitivity that the *XMM–Newton* optics offer. In our sample, the Compton-thick nature is confirmed for all objects, except NGC 5005 ($N_{\rm H} \simeq 1.5 \times 10^{23}$ cm^{-2}) and – marginally – NGC 5643 (Guainazzi et al. 2004a;

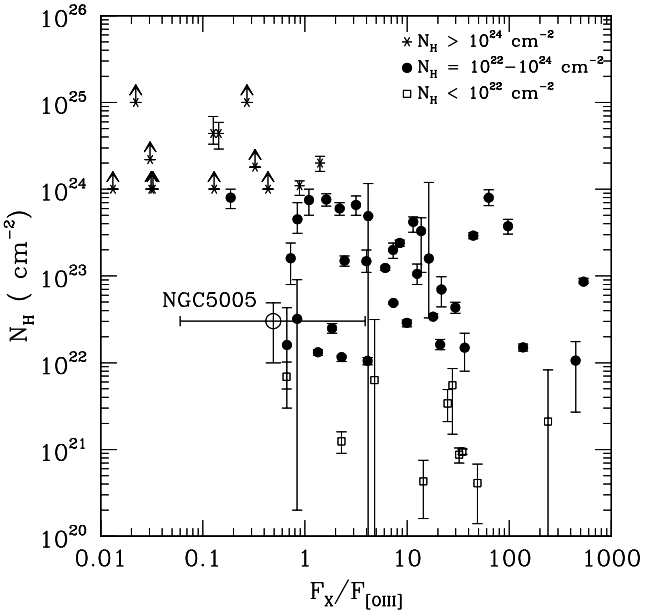

Figure 7. Absorbing column density N_H versus 2–10 keV to O [III] flux ratio for the sample of Seyfert 2 galaxies after Bassani et al. (1999). The empty circle indicates the location corresponding to NGC 5005 for the column density observed by *XMM–Newton*, and the O[III] fluxes reported in the literature (details in text).

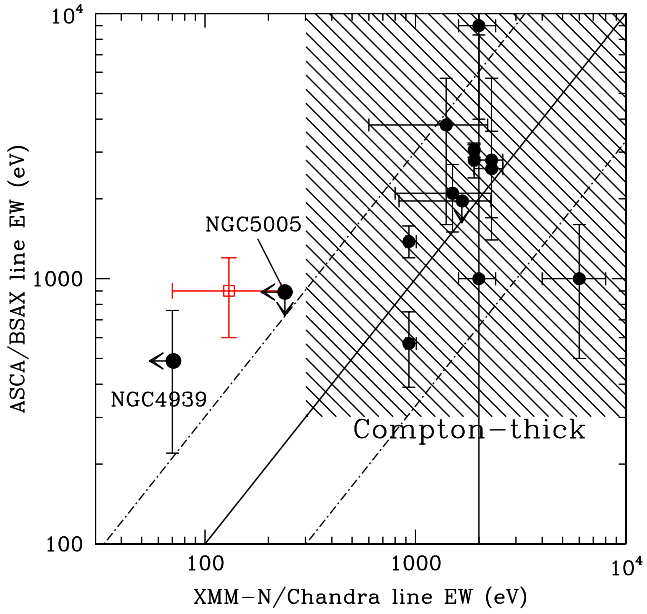

Figure 8. EW of the $K\alpha$ neutral iron fluorescent emission line measured by *ASCA*/*BeppoSAX* as a function of the same quantity measured by *Chandra*/*XMM–Newton*. The locus corresponding to 'static' Compton-thick objects is indicated by the shaded area. Filled circles: objects of our sample; open square: UGC 4203, the prototypical 'Phoenix Galaxy' (Guainazzi 2002). The solid (dashed) line represents the identity (±factor 3) locus.

$N_H = 6–10 \times 10^{23}$ cm^{-2}), apart from NGC 4939, obviously. This is a potentially important result, as it underlines the perspective to extend the search for Compton-thick objects at higher redshift (Fabian, Wilman & Crawford 2002). Although classification of an individual object may be subject to uncertainties even when large EW iron lines are detected, the method is robust.

6.2 The moderately unstable temper of heavily obscured AGN

The scope of this paper is comparing the X-ray spectral properties of a complete, unbiased sample of Compton-thick Seyfert 2 galaxies observed with *Chandra* and *XMM–Newton* with prior measurements. The main scientific goal is to estimate the rate of transitions between transmission- and reprocessing-dominated spectral states.

These transitions were serendipitously discovered on a few nearby active nuclei, once a larger data base of X-ray observations allowed us some knowledge of the X-ray history of a wider sample of AGN. These transitions affect Seyfert 2 galaxies (NGC 2992, Gilli et al. 2000; NGC 1365, Iyomoto et al. 1997; Risaliti et al. 2000; UGC 4203, Guainazzi et al. 2001; NGC 6300, Guainazzi 2002), as well as other AGN (NGC 4051, Guainazzi et al. 1998; Uttley et al. 1999; PG 2112+059, Gallagher et al. 2004). It has been claimed that variability of the absorbing column density by a factor 50 ± 30 per cent on time-scales $\leqslant$1 yr is common in obscured AGN (Risaliti, Elvis & Nicastro 2002). In one of the best-monitored cases (NGC 3227, Lamer, Uttley & McHardy 2003), the symmetric profile of the absorption light curve clearly suggests an interpretation in terms of line-of-sight crossing by an individual cloud. The transitions we are discussing in this paper, however, represent a different phenomenology, whereby the apparent variation of the absorbing column density is of at least one order of magnitude, and the state corresponding to the lower X-ray flux is fully reprocessing-dominated.

The main conclusion of this study is summarized in Fig. 8, where we use the $K\alpha$ iron line EW – measured by *BeppoSAX*/*ASCA* and *Chandra*/*XMM–Newton* – as a hallmark for bona fide Compton-thick AGN. Only narrow or unresolved components corresponding to neutral or mildly ionized iron transitions have been used in the calculation of the EWs shown in Fig. 8. We do not consider the contribution of the Compton shoulder, which is likely to be $\lesssim$20 per cent in most cases (Matt 2002). The locus corresponding to Compton-thick objects is conservatively bordered by the line EW $\equiv$ 300 eV, corresponding to the brightest emission line produced by transmission through a Compton-thin screen, covering a 2π solid angle (Leahy & Creighton 1993). Out of the 10 Compton-thick Seyferts discussed in this paper, we find evidence for only one transition: NGC 4939. This implies that a typical time-scale for these transitions should be $\simeq$50 yr, on the basis of the average separation between the *ASCA*/*BeppoSAX* and the closest *Chandra*/*XMM–Newton* observations. Of course, given the size of our sample, this has to be regarded as no more than an order-of-magnitude estimate. However, it is consistent with previous determinations, based on inhomogeneous and incomplete samples.

The origin of the spectral changes occurring when an AGN transforms its appearance from a transmission- to a reprocessing-dominated state is still not fully elucidated. In principle, high-quality, high-resolution measurements, following the onset of the variability or the AGN recovery after a prolonged off-state, should be decisive.

In NGC 6300 and 2992 we have the strongest evidence that transitions from transmission- to reprocessing-dominated states are due to a change of the optical path through which the nucleus is being observed, due to a temporary interruption of the nuclear activity. In NGC 6300 this is suggested by the very large Compton-reflection continuum observed by *BeppoSAX* (Guainazzi 2002). In NGC 2992, the history of the X-ray emission is comparatively well sampled. The X-ray flux decreased by about a factor of 20 from the first HEAO-1 detection in the early 1980s, up to the 1994 *ASCA* observation, just to experience a factor $\simeq$15 recovery by 1999 (Gilli et al. 2000). To these two cases, we might add the large dynamical range of the

NGC 5643 AGN X-ray output (Guainazzi et al. 2004b), a promising transition candidate. Unfortunately our knowledge of the X-ray history of NGC 4939 and UGC 4203 is too poor for us to be able to draw any final conclusions on this issue. Recently Ohno et al. (2004) proposed a change by a factor >5 of the absorber column density as the most likely explanation in the latter. On the other hand, multiple X-ray observations of optically defined samples of unobscured AGN have not detected a significant rate of large historical X-ray flux variations (compare, for instance, Laor et al. 1997; George et al. 1998; Porquet et al. 2004). When one is dealing with X-ray unobscured AGN a bias toward the brightest, less obscured object may prevent us from discovering the fraction of X-ray unobscured counterparts to our transient Compton-thick Seyferts. However, this may also suggest an alternative interpretation in terms of changes in the properties of line-of-sight gas. This scenario will be investigated in the next section.

6.3 The recovery of fossil AGN as a probe of the circumnuclear medium

Transmission- to reprocessing-dominated transitions can be used to probe some properties of the gas in the nuclear environment in highly obscured AGN. The method – based on Monte Carlo simulations – is described by Matt et al. (2003b). The application of this method to the five known transitions is summarized in Fig. 9, where we show the 2–4 keV versus 4–10 keV flux softness ratio for the Compton-reflection component in the reprocessing-dominated state against the measured column density in the transmission-dominated state.[3] The solid line represents the expected correlation according to simulations. In the *ASCA* observation of NGC 2992, and possibly in UGC 4203, the spectrum observed during a reprocessing-dominated state is too hard to be due to Compton-reflection by matter with the same column density as measured by the soft photoelectric cut-off during transmission-dominated states. A similar argument can be applied to NGC 6300, on the basis of its X-ray spectrum above 10 keV (Guainazzi 2002; Matt et al. 2003b). The gas responsible for line-of-sight absorption should therefore be different in density from the gas responsible for reflection, the latter being most likely located at the far inner side of the molecular 'torus'. This may be explained by a largely inhomogeneous compact (i.e. 1 pc) nuclear absorber (Ohno et al. 2004), or by Compton-thin absorption occurring on much larger scales than the nuclear 'torus', e.g. in dusty regions associated with starburst formation (Weaver 2001), or with the host galaxy (Maiolino & Rieke 1995; Malkan, Gorijn & Tam 1998). An extension of the Seyfert unified scenario, which encompasses the latter possibility, is discussed by Matt (2000). It is also noteworthy that in three out of five cases the softness ratio in Fig. 9 is softer than expected by a pure Compton-reflection spectrum even in the reprocessing-dominated states. This suggest a still non-negligible contamination by a softer component, e.g. a not fully 'switched-off' AGN continuum. This possibility is confirmed by our reanalysis of the *BeppoSAX* observation of NGC 2992, the X-ray brightest among the objects displayed in Fig. 9, where the recovery of the AGN is witnessed by a comparatively small value of the normalization ratio between the reflected and the transmitted component [$R \simeq 4\ (\Omega/2\ \pi)$] with respect to a bare Compton-reflection dominated state.

In summary, the spectral properties of transmission- to reprocessing-dominated transitions indicate that obscuring matter in AGN is far from being homogeneous in space or time. Yet, one cannot discard the idea of a compact but inhomogeneous parsec-scale torus (Antonucci 1993), or disc outflow (Elvis 2000). Such inhomogeneities might ultimately be responsible for these transitions. However, the fact that photoionized- or starburst-dominated soft X-ray emission in several Seyfert 2 galaxies is absorbed as well (Iwasawa & Comastri 1998; Matt et al. 2001, 2003a), alongside our knowledge of the X-ray history in NGC 6300 and, above all, NGC 2992, suggests that an important contribution to X-ray obscuration comes from matter associated to the host galaxy, beyond the innermost parsec around the central engine.

[3] We consider here the first *BeppoSAX* observation for NGC 2992, performed in 1997.

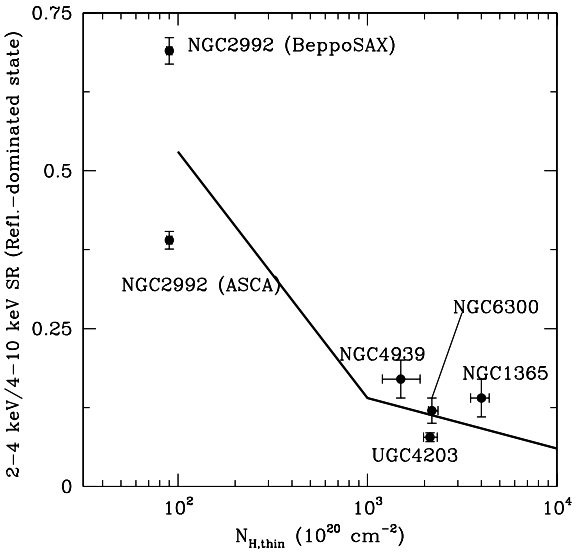

Figure 9. 2–4 keV to 4–10 keV flux softness ratio (SR) in the reprocessing-dominated state against the N_H measured in transmission-dominated states for the five objects, where a transition between the two states has been reported in the literature (cf. Section 6.2), plus NGC 4939 (this paper). The *solid line* represents the expected correlation on the basis of Monte Carlo simulations of Compton-reflection spectra (Matt et al. 2003b).

6.4 The origin of the soft X-ray emission

Our programme was not specifically tuned to investigate the origin of the soft X-ray emission in our sample. The answers that we get from the data on this issue are therefore inevitably ambiguous in almost all cases. The only exception is NGC 5005 (the only non-Compton-thick source in the sample). In this case, the soft X-ray emission is clearly extended on scales comparable with the optical size of the galaxy, and roughly aligned with its main axis, or with an inner arm ultraviolet (UV) structure. For all the other cases, the two proposed scenarios are equally viable on the basis of the EPIC data alone. Whenever high-resolution spectroscopic data are available, soft X-rays appear to be dominated by emission lines following photoionization and photoexcitation by the primary AGN emission (Bianchi, Matt & Iwasawa 2001; Sambruna et al. 2001; Kinkhabwala et al. 2002), with little or no contribution by nuclear starbursts. On the other hand, the 0.5–4.5 keV X-ray luminosities are generally consistent with the correlation with the far infrared (FIR) luminosity empirically determined by David, Jones & Forman (1992) on a large sample of starburst-dominated galaxies (Turner et al. 1997; Maiolino et al. 1998; Fig. 10), the only discrepant objects being NGC 4939 and 4945.

This, however, holds also for objects (such as the Circinus Galaxy) for which it is unlikely that soft X-rays are dominated by

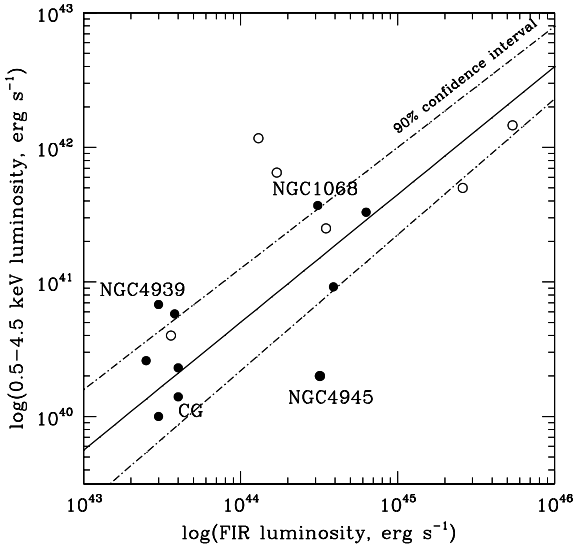

Figure 10. FIR luminosity (as defined in David et al. 1992) against the 0.5–4.5 keV luminosity for the Compton-thick objects of our sample (filled dots), and the remaining Compton-thick Seyfert 2 galaxies of Bassani et al. (1999). The solid line indicates the empirical correlation found by David et al. (1992) for starburst galaxies; the dashed lines indicates the 90 per cent confidence level on this correlation. 'CG': the Circinus Galaxy.

starburst. On the other hand, high-resolution imaging of NGC 4945 with *Chandra* shows that soft X-rays are likely to be dominated by thermal emission from starbursts, alongside a starburst mass-loaded superwind (Schurch et al. 2002). While we refer to Guainazzi et al. (2004a) for a more detailed discussion on this point, we conclude for the time being that a thorough determination of the physical properties of the plasma dominating the soft X-rays in obscured AGN requires deep exposures with high-resolution detectors, which are currently possible only on a limited number of objects.

7 CONCLUSIONS

The main result of this paper is the estimate of the occurrence rate of transmission- to reprocessing-dominated state transitions, on the most unbiased and complete existing sample of Compton-thick Seyfert 2 galaxies (cf. Fig. 8). We have discovered one (new) transition out of a sample of 11 bona fide Compton-thick objects, with an average time span between pre- and post-*XMM–Newton* and *Chandra* launch observations of about 5 yr. The statistics is still too small to determine anything more accurate than an order-of-magnitude estimate for the occurrence rate. Bearing this caveat in mind, it seems that once or twice every century we might be forced to change our X-ray absorption classification for each highly obscured AGN.

With respect to the mechanism responsible for these transitions, our results are consistent with the discussion in Matt et al. (2003b). Although an explanation in terms of varying line-of-sight column density cannot be ruled out, the fact that in the best-studied cases these transitions are associated with large (>10) fluctuations of the AGN X-ray output suggests that they are due to a change of the optical path through which we observe the nucleus. For the transition specifically discussed in this paper – NGC 4939 – the factor of 2 variation of the observed 2–10 keV band flux hides a larger variation of the AGN intrinsic power, as its true luminosity in the reprocessing-dominated state is unknown. If this is the correct interpretation, the transition occurrence rate translates immediately into a duty cycle of the AGN phenomenon in the local Universe.

Independently of the ultimate mechanism responsible for these transitions, comparison of their spectral properties with Monte Carlo simulations demonstrates that obscuring gas in absorbed AGN cannot be distributed in a space- or time-homogeneous structure. Again, a compact but inhomogeneous torus cannot be ruled out. However, there is mounting evidence that gas in regions of intense star formation and dust in the host galaxy play a major role, and might be ultimately responsible for the bulk of Compton-thin X-ray absorption in AGN.

ACKNOWLEDGMENTS

This paper is based on observations obtained with *XMM–Newton*, an ESA science mission with instruments and contributions directly funded by ESA Member States and the USA (NASA). This research has made use of data obtained through the High Energy Astrophysics Science Archive Research Center Online Service, provided by the NASA/Goddard Space Flight Center and of the NASA/IPAC Extragalactic Database (NED) which is operated by the Jet Propulsion Laboratory, California Institute of Technology, under contract with the National Aeronautics and Space Administration. GM acknowledges financial support from MIUR grant COFIN-03-02-23. Careful reading, and insightful suggestions by an anonymous referee are gratefully acknowledged.

REFERENCES

Antonucci R., 1993, ARA&A, 31, 473
Bassani L., Dadina M., Maiolino R., Salvati M., Risaliti G., della Ceca R., Matt G., Zamorani G., 1999, ApJS, 121, 473
Bennett C. L. et al., 2003, ApJS, 148, 1
Bianchi S., Matt G., Fiore F., Fabian A. C., Iwasawa K., Nicastro F., 2002, A&A, 396, 793
Bianchi S., Matt G., Iwasawa K., 2001, MNRAS, 322, 669
Brinkman A. C., Kaastra J. C., van der Meer R. J. L., Kinkhabwala A., Behar E., Kahn S., Paerels F. B. S., Sako M., 2002, A&A, 396, 761
Colbert E. J. M., Weaver K. A., Krolik J. H., Mulchaey J. S., Mushotzky R. F., 2002, ApJ, 581, 182
Comastri A., 2004, in Barger A. J., ed., Astrophys. Space Sci. Library Vol. 308, Supermassive Black Holes in the Distant Universe. Kluwer, Dordrecht, p. 245
Dahari O., De Robertis M. E., 1988, ApJS, 67, 249
David L. P., Jones C., Forman W., 1992, ApJ, 388, 82
Done C., Madejski G. M., Smith D. A., 1996, ApJ, 463, L63
Elvis M., 2000, ApJ, 545, 63
Fabian A. C., Wilman R. J., Crawford C. S., 2002, MNRAS, 329, L18
Gallagher S. C., Brandt W. N., Wills B. J., Charlton J. C., Chartas G., Laor A., 2004, ApJ, 603, 425
George I. M., Turner T. J., Netzer H., Nandra K., Mushotzky R. F., Yaqoob T., 1998, ApJS, 114, 73
Gilli R., Maiolino R., Marconi A., Risaliti G., Dadina M., Weaver K. A., Colbert E. J. M., 2000, A&A, 355, 485
Guainazzi M., 2002, MNRAS, 329, L13
Guainazzi M. et al., 1998, MNRAS, 301, L1
Guainazzi M., Matt G., Brandt W. N., Antonelli L. A., Barr P., Bassani L., 2000a, A&A, 356, 463
Guainazzi M., Molendi S., Vignati P., Matt G., Iwasawa K., 2000b, New Astron., 5, 235
Guainazzi M., Matt G., Fiore F., Perola G. C., 2001, A&A, 388, 787
Guainazzi M., Rodriguez-Pascual P., Fabian A. C., Iwasawa K., Matt G., 2004a, MNRAS, 355, 297
Guainazzi M., Rodriguez-Pascual P., Fabian A. C., Iwasawa K., Matt G., Fiore F., 2004b, in Mujica R., Maiolino R., eds, Proc. Conf.

Multiwavelength AGN Surveys. World Scientific, Singapore, in press (astro-ph/0404031)
Ho L. C., Filippenko A. V., Sargent W. L. W., 1997, ApJS, 112, 315
Kinkhabwala A. et al., 2002, ApJ, 575, 732
Jansen F. et al., 2001, A&A, 365, L1
Ishihara Y., Makai N., Itomoto N., Makishima K., Diamonds P., Hall P., 2001, PASJ, 53, 215
Iyomoto N., Makishima K., Fukazawa Y., Tashiro M., Ishisaki Y., 1997, PASJ, 49, 425
Iwasawa K., Comastri A., 1998, MNRAS, 297, 1219
Iwasawa K., Fabian A. C., Matt G., 1997, MNRAS, 289, 443
Iwasawa K., Maloney P. R., Fabian A. C., 2002, MNRAS, 336, L71
Iwasawa K., Wilson A. S., Fabian A. C., Young A. J., 2003, MNRAS, 345, 369
Lamer G., Uttley P., McHardy I. M., 2003, MNRAS, 342, L41
Laor A., Fiore F., Elvis M., Wilkes B. J., McDowell J. C., 1997, ApJ, 477, 93
Leahy D. A., Creighton J., 1993, MNRAS, 263, 314
Levenson N. A., Krolik J. H., Życki P. T., Heckman T. M., Weaver K. A., Awaki H., Terashima Y., 2002, ApJ, 573, L81
Levenson N. A., Weaver K. A., Heckman T. M., Awaki H., Terashima Y., 2004, ApJ, 602, 135
Madejski G., Zycki P., Done C., Valinia A., Blanco P., Rothschild R., Turek B., 2000, ApJ, 535, L87
Magdziarz P., Zdziarski A. A., 1995, MNRAS, 273, 837
Maiolino R., Rieke G. H., 1995, ApJ, 454, 95
Maiolino R., Salvati M., Bassani L., Dadina M., della Ceca R., Matt G., Risaliti G., Zamorani G., 1998, A&A, 338, 781
Malkan M. A., Gorijn V., Tam R., 1998, ApJS, 117, 25
Matt G., 2000, A&A, 335, L31
Matt G., 2002, MNRAS, 337, 147
Matt G. et al., 1996, MNRAS, 281, L69
Matt G. et al., 1997a, A&A, 325, L13
Matt G., Fabian A. C., Reynolds C., 1997b, MNRAS, 289, 175
Matt G. et al., 1999, A&A, 341, L39
Matt G., Fabian A. C., Guainazzi M., Iwasawa K., Bassani L., Malaguti G., 2000, MNRAS, 318, 173
Matt G., Guainazzi M., Perola G. C., Fiore F., Nicastro F., Cappi M., Piro L., 2001, A&A, 377, L31
Matt G., Bianchi S., Guainazzi M., Brandt W. M., Fabian A. C., Iwasawa K., Perola G. C., 2003a, A&A, 399, 519
Matt G., Guainazzi M., Maiolino R., 2003b, MNRAS, 342, 422
Matt G., Bianchi S., Guainazzi M., Molendi S., 2004, A&A, 414, 155
Mewe R., Gronenschild E. H. B. M., van der Oord G. H. J., 1985, A&AS, 62, 197
Molendi S., Bianchi S., Matt G., 2003, MNRAS, 343, L1
Ohno M., Fukazawa Y., Iyomoto N., 2004, PASJ, 56, 425
Porquet D., Reeves J. N., O'Brien P., Brinkmann W., 2004, A&A, 422, 85
Risaliti G., Maiolino R., Salvati M., 1999, ApJ, 522, 157
Risaliti G., Maiolino R., Bassani L., 2000, A&A, 356, 33
Risaliti G., Elvis M., Nicastro F., 2002, ApJ, 571, 234
Sambruna R., Netzer H., Kaspi S., Brandt W. N., Chartas G., Garmire G. P., Nousek J. A., Weaver K. A., 2001, ApJ, 546, L13
Schurch N. J., Roberts T. P., Warwick R., 2002, MNRAS, 335, 24
Shuder J. M., Osterbrock D. E., 1981, ApJ, 250, 55
Strüder L. et al., 2001, A&A, 365, L18
Turner T. J., George I. M., Nandra K., Mushotzky R. F., 1997, ApJS, 113, 23
Turner M. J. L. et al., 2001, A&A, 365, L27
Ueno S., Mushotzky R. F., Koyama K., Iwasawa K., Awaki H., Hayashi I., 1994, PASJ, 46, L71
Uttley P., McHardy I., Papadakis I. E., Guainazzi M., Fruscione A., 1999, MNRAS, 307, L6
Weaver K., 2001, in Knapen J. H., Beckman J. E., Shlosman I., Mahoney T. J., eds, ASP Conf. Ser. Vol. 249, The Central Kiloparsec of Starbursts and AGN: the La Palma Connection. Astron. Soc. Pac., San Francisco, p. 389
Wilson A. S., Elvis M., Lawrence A., Bland-Hawthorn J., 1992, ApJ, 391, L75

This paper has been typeset from a TEX/LATEX file prepared by the author.